Rate Constants for $CH_3 + O_2 \rightarrow CH_3O + O$ at High Temperature and Evidence for $H_2CO + O_2 \rightarrow HCO + HO_2$

J. V. Michael,* S. S. Kumaran,† and M.-C. Su‡

Chemistry Division, Argonne National Laboratory, Argonne, Illinois 60439

Received: March 17, 1999; In Final Form: May 17, 1999

The reaction of CH_3 with O_2 has been studied in a reflected shock tube apparatus between 1600 and 2100 K. CH_3 was prepared from the fast thermal decomposition of CH_3I, and O atom atomic resonance absorption spectrometry (ARAS) was used to observe absolute $[O]_t$. $[CH_3I]_0$ was sufficiently low so that most secondary reactions were negligible, allowing for unambiguous determination of the rate constant for $CH_3 + O_2 \rightarrow CH_3O + O$. The rate constant expression for this reaction derived to match the experimental data is $k = (3.90 \pm 0.40) \times 10^{-11} \exp(-16858 \pm 1127\ \mathrm{K}/T)\ \mathrm{cm^3\ molecule^{-1}\ s^{-1}}$. To explain O atom concentration buildup at longer times, a fast reaction between H_2CO and O_2 was postulated. Rate constants for this process were derived by fitting the long-time O atom profiles. Last, the four-center reaction $CH_3 + O_2 \rightarrow CH_2O + OH$ was found to be of negligible importance over the temperature range of the study.

Introduction

The reaction of CH_3 with O_2 is one of the most important reactions in hydrocarbon combustion. This issue has of course been recognized for over 50 years, and the work on the reaction is extensive as shown by the fact that there are 107 references to it in the NIST database.[1] Three elementary reactions are possible:

$$CH_3 + O_2\ (+M) \rightarrow CH_3O_2\ (+M) \quad (1)$$

$$\rightarrow CH_2O + OH \quad (2)$$

$$\rightarrow CH_3O + O \quad (3)$$

Reactions 2 and 3 are forward dissociation channels from the initially formed vibrationally hot methylperoxy radical in competition with stabilization (reaction 1). As temperature increases, the back process, reaction −1, also becomes important in an RRKM sense, decreasing the overall rate of reaction 1 to negligible values above ∼1500 K and below ∼400 Torr. On the other hand, reactions 2 and 3 have activation barriers, and these channels open only at higher temperatures and dominate reaction 1. Hence, under the present high-temperature conditions, reactions 2 and 3 are the important reactions.

The branching ratio of reactions 2 and 3 has been a perplexing problem for a long time. Recently, Yu, Wang, and Frenklach[2] have thoroughly discussed the earlier data on both reactions and have noted that there is agreement between the various values for reaction 3 (within a factor of 3), but the spread in values for reaction 2 is over an order of magnitude. These workers shock-heated methane−oxygen mixtures and spectroscopically measured both $[OH]_t$ and $[CO]_t$. They then used optimization techniques and GRI-Mech[3] to fit the data, the most important CH_3 oxidation rate processes being reactions 2 and 3. They report

$$k_2 = 3.07 \times 10^{-12} \exp(-10224\ \mathrm{K}/T)\ \mathrm{cm^3\ molecule^{-1}\ s^{-1}} \quad (4)$$

and

$$k_3 = 4.90 \times 10^{-11} \exp(-15340\ \mathrm{K}/T)\ \mathrm{cm^3\ molecule^{-1}\ s^{-1}} \quad (5)$$

For reaction 2, they showed that the earlier data could be separated into two distinct sets, one suggesting high values[4−11] and the other suggesting low values for k_2.[12−19] Their result, eq 4, clearly suggests that the low values are preferred. With regard to reaction 3, the results were more uniform. Except for the data of Saito et al.,[10] the earlier values[11,14−17,20,21] agreed with eq 5 to within a factor of 2. The results for reaction 3 would then seem to be consistent; however, in a recent report,[19] Braun-Unkhoff et al. have indicated that their $[OH]_t$ measurements required k_3 to be about one-half to one-third of eq 5. Similarly, OH and CH_3 profile results by Tischer et al.[22] have given values for k_3 that are lower than eq 5 by about one-half. Hence, we have concluded that the situation is still perplexing, and this realization has prompted the present study.

In the present work, the formation rates of O atoms are measured behind reflected shock waves using the atomic resonance absorption spectrometry (ARAS) technique. The experiments are similar to those of Bhaskaran et al.[14] and Klatt et al.[17] except that O atom detection is about 5 times more sensitive than in these two earlier studies. This is important because the complications from secondary reactions can be suppressed by observing O atom production at lower reactant concentrations.

Experimental Section

The present experiments were performed with previously described equipment,[23] and therefore, only a brief description

* To whom correspondence should be addressed. Address: D-193, Bldg. 200, Argonne National Laboratory Argonne, IL 60439. Phone: (630) 252-3171. Fax: (630) 252-4470. E-mail: Michael@anlchm.chm.anl.gov.

† Present address: Cabot Corporation, 700 E. US Highway 36, Tuscola, IL 61953.

‡ Faculty Research Participant, Department of Educational Programs, Argonne. Permanent address: Department of Chemistry, Butler University, Indianapolis, IN 46208.

10.1021/jp9909457 CCC: $18.00
Published on Web 07/09/1999

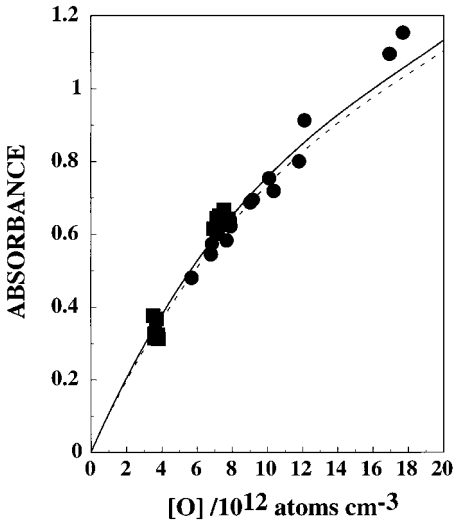

Figure 1. Curve-of-growth determination for O atom ARAS: (■) from ref 25 [O] data based on the unimolecular decomposition of N_2O; (●) [O] derived from a simulation using the mechanism given in Table 1. (ABS) is the experimentally determined absorbance (see text).

of the system, along with those features unique to the current experimental procedures, will be presented here.

Apparatus. The apparatus consists of a 7 m (4 in. o.d.) 304 stainless steel tube separated from the He driver chamber by a 4 mil unscored 1100-H18 aluminum diaphragm. The tube was routinely pumped between experiments to less than 10^{-8} Torr by an Edwards Vacuum Products model CR100P packaged pumping system. The velocity of the shock wave was measured with eight equally spaced pressure transducers (PCB Piezotronics, Inc., model 113A21) mounted along the downstream part of the test section of the shock tube and recorded with a 4094C Nicolet digital oscilloscope. Temperature and density in the reflected shock wave regime were calculated from this velocity. This procedure has been given previously, and corrections for boundary layer perturbations have been applied.[23,24] The digital oscilloscope was triggered by pulses derived from the last velocity gauge signal. The photometer system was radially located 6 cm from the end plate. All optics were made from MgF_2. The resonance lamp beam intensity was measured by an EMR G14 solar blind photomultiplier tube and recorded with the oscilloscope.

O Atom ARAS. The technique used for the detection of the transient O atoms formed in reaction 3 is atomic resonance absorption spectroscopy (ARAS). In earlier work,[25] O atom curves-of-growth were determined for two different resonance lamp conditions: (1) $X_{O_2} = 1 \times 10^{-3}$ in 1.8 Torr of purified grade He and (2) no added O_2 in purified grade He, both operating at 50 W microwave power to give an effective lamp temperature of 490 K.[26] Method 2 relies on the O_2 impurity in the He tank and has a less reversed line shape than method 1; however, method 1 was used in the present work because the signal-to-noise ratio is better. The nonoverlapping 130.2, 130.4, and 130.6 nm triplet resonance lines are isolated with a CaF_2 window (transmitting at wavelengths greater than 125 nm), and the fraction of the light that is resonance radiation is determined by using an O atom atomic filter section in front of the lamp as described previously.[25]

In the earlier work,[25] O atom concentration calibration was carried out using the thermal decomposition of N_2O. These measurements are shown as solid squares in Figure 1. From these data alone the derived curve-of-growth (COG), calculated from atomic resonance line absorption theory,[25−27] is reproduced as the dashed line in Figure 1. We found that the COG for the moderately reversed source was not strongly dependent on temperature, as shown by the data and line absorption calculations. In the present work, the relationship between [O] and absorbance (ABS) ((ABS) ≡ $-\ln(I/I_0)$ where I_0 and I refer to initial and transmitted resonance light intensities, respectively) was determined under slightly lower temperature conditions than before.[25] The present method utilizes the reaction

$$H + O_2 \rightarrow OH + O \qquad (6)$$

at low $[H]_0$ where the H atoms are produced from the fast thermal decomposition of C_2H_5I.[28,29] The pertinent mechanism is given in Table 1 along with well-established rate constants for all processes. Experiments have been performed by varying $[C_2H_5I]_0$ in excess O_2, and absorption profiles were measured at several temperatures. The absorption profiles rapidly decreased to a near-constant level. [O] was then simulated over the time necessary to obtain near-constant absorption by numerically integrating the mechanism of Table 1. The conditions of the experiments are shown in Table 2. For 14 experiments in the table, the simulated [O] is listed along with the measured (ABS), and these values are subsequently plotted in Figure 1 (closed circles) along with the earlier results from the N_2O decomposition study.[25] It should be noted that reactions 5 and 6 in Table 1 are negligible, contributing less than 0.5% to [O]. The profile is mostly affected by (a) the branching ratio of reactions 1 and 2 and (b) by the H + O_2 reaction. The maximum contribution to [O] from the OH + OH (reaction 4 in Table 1) at the highest temperature and $[C_2H_5I]_0$ is less than 5%.

TABLE 1: Mechanism Used for Determining (ABS) against [O] from the H + O_2 Reaction Using C_2H_5I as a Source of H Atoms[a]

1. C_2H_5I (+M) → C_2H_4 + H + I (+M), $k_1 = 6.34 \times 10^9 \exp(-15894\ \mathrm{K}/T)$[b]
2. C_2H_5I (+M) → C_2H_4 + HI (+M), $k_2 = 0.15 \times k_1$[b]
3. H + O_2 → OH + O, $k_3 = 1.62 \times 10^{-10} \exp(-7474\ \mathrm{K}/T)$[c]
4. OH + OH → O + H_2O, $k_4 = 7.19 \times 10^{-21} T^{2.7} \exp(1251\ \mathrm{K}/T)$[c]
5. H + HI → H_2 + I, $k_5 = 7.87 \times 10^{-11} \exp(-330\ \mathrm{K}/T)$[d]
6. I + H_2 → HI + H, $k_6 = 2.81 \times 10^{-10} \exp(-16930\ \mathrm{K}/T)$[d]

[a] All rate constants are in $\mathrm{cm^3\ molecule^{-1}\ s^{-1}}$ except for reactions 1 and 2, which are in $\mathrm{s^{-1}}$. [b] Reference 28. [c] Reference 30. [d] Reference 31.

TABLE 2: Data for O Atom Curve-of-Growth Determination

P_1/ Torr	M_s[a]	ρ_5[b]/ (10^{18} cm^{-3})	T_5[b]/K	$[C_2H_5I]_0$[c]/ cm^{-3}	$[O]_{sim}$[c]/ cm^{-3}	(ABS)
$X_{C_2H_5I} = 6.266 \times 10^{-6}$, $X_{O_2} = 1.763 \times 10^{-3}$						
10.94	2.580	2.163	1656	[c]1.356 (13)	1.211 (13)	0.913
8.84	2.618	1.772	1702	1.110 (13)	1.010 (13)	0.755
7.98	2.623	1.602	1707	1.004 (13)	0.902 (13)	0.688
7.02	2.555	1.376	1627	0.862 (13)	0.789 (13)	0.623
6.09	2.589	1.208	1667	0.757 (13)	0.679 (13)	0.545
5.01	2.612	1.002	1694	0.628 (13)	0.569 (13)	0.481
15.90	2.600	3.147	1673	1.972 (13)	1.769 (13)	1.154
15.95	2.489	3.035	1547	1.902 (13)	1.694 (13)	1.096
10.97	2.431	2.046	1485	1.282 (13)	1.180 (13)	0.801
9.81	2.417	1.819	1470	1.140 (13)	1.036 (13)	0.720
8.63	2.474	1.639	1534	1.027 (13)	0.916 (13)	0.695
7.49	2.394	1.375	1445	0.862 (13)	0.767 (13)	0.584
7.57	2.460	1.430	1519	0.896 (13)	0.787 (13)	0.640
6.55	2.594	1.302	1673	0.816 (13)	0.684 (13)	0.574

[a] The error in measuring the Mach number, M_s, is typically 0.5−1.0% at the one standard deviation level. [b] Quantities with the subscript 5 refer to the thermodynamic state of the gas in the reflected shock region. [c] Parentheses denote the power of 10.

TABLE 3: High-Temperature Rate Data for CH_3 Oxidation by O_2

P_1/ Torr	M_s[a]	ρ_5[b]/ (10^{18} cm^{-3})	T_5[b]/K	k_3[c,d]/ (cm^3 s^{-1})	k_{16}[c,d]/ (cm^3 s^{-1})
$X_{CH_3I} = 2.482 \times 10^{-6}$, $X_{O_2} = 1.056 \times 10^{-1}$					
5.92	2.682	1.333	1644	1.95 (−15)	2.0 (−15)
5.96	2.823	1.410	1802	3.00 (−15)	3.0 (−15)
5.92	3.055	1.502	2078	1.20 (−14)	8.0 (−14)
7.48	2.959	1.847	1962	8.00 (−15)	2.0 (−14)
7.46	3.045	1.887	2066	1.04 (−14)	5.0 (−14)
$X_{CH_3I} = 1.592 \times 10^{-6}$, $X_{O_2} = 5.822 \times 10^{-2}$					
10.96	2.865	2.517	1916	6.50 (−15)	1.5 (−14)
10.79	2.998	2.574	2083	1.70 (−14)	7.0 (−14)
10.95	3.018	2.626	2109	1.60 (−14)	7.0 (−14)
10.99	2.960	2.594	2035	1.00 (−14)	5.0 (−14)
10.93	2.824	2.479	1867	4.00 (−15)	1.5 (−14)
10.91	2.688	2.357	1712	1.65 (−15)	4.0 (−15)
10.96	2.597	2.290	1608	1.40 (−15)	1.0 (−15)
10.97	2.715	2.392	1744	2.20 (−15)	4.0 (−15)
10.99	2.647	2.340	1665	1.50 (−15)	2.0 (−15)
10.98	2.776	2.444	1815	2.20 (−15)	5.0 (−15)
10.95	2.909	2.539	1977	9.50 (−15)	1.5 (−14)
10.93	2.971	2.579	2055	1.00 (−14)	6.0 (−14)
10.93	2.999	2.599	2091	9.00 (−15)	5.0 (−14)

[a] The error in measuring the Mach number, M_s, is typically 0.5−1.0% at the one standard deviation level. [b] Quantities with the subscript 5 refer to the thermodynamic state of the gas in the reflected shock region. [c] Fitted rate constants for reactions 3 and 16 of Table 4 (see text). [d] Parentheses denote the power of 10.

From Figure 1, the earlier data from the N_2O decomposition agree with the results based on the Table 1 mechanism within experimental error. We showed earlier that our H atom ARAS calibration methods[26] agreed with independent Cl [32] and I atom[33] ARAS results. The present results are in fact a calibration between H and O atom ARAS methods and, as a result, corroborate the Table 1 mechanism and, particularly, the branching ratio between reactions 1 and 2. Last, we have parametrically applied line absorption calculations[25−27] to the composite set (the present and earlier data[25]), allowing only [O] in the resonance lamp to vary. This affects the extent of reversal and therefore the sensitivity for detection. A minimum one standard deviation of ±6.5% was found between calculations and the composite data points if the mole fraction of O atoms in the lamp was 5.2×10^{-4} (i.e., 26% O_2 dissociation). The resultant COG is plotted as the solid line in Figure 1. The differences between the new and earlier[25] (dashed line) COG are insignificant. Hence, because of the above-mentioned consistencies between calibration techniques, we consider the [O] analysis in the present work to be accurate to within about ±10%.

Kinetics Experiments. Eighteen kinetics experiments were carried out between 1608 and 2091 K under the conditions shown in Table 3. The experiments were similar to the above-mentioned calibration determinations, the only difference being that C_2H_5I was replaced by CH_3I. It was of course necessary to increase $[O_2]$ substantially, since reaction 3 is known to be much slower than reaction 6. O atom formation rates must exclusively arise from the reactions of CH_3 radicals formed from the fast dissociation of CH_3I,[33] since under similar circumstances we have already shown that $I + O_2$ is negligibly slow over the time period of the experiments.[34]

Gases. High-purity He (99.995%), used as the driver gas, was from Air Products and Chemicals, Inc. Scientific grade Kr (99.999%), the diluent gas in reactant mixtures, was from Spectra Gases, Inc. The ~10 ppm impurities (N_2, 2 ppm; O_2, 0.5 ppm; Ar, 2 ppm; CO_2, 0.5 ppm; H_2, 0.5 ppm; CH_4, 0.5 ppm; H_2O, 0.5 ppm; Xe, 5 ppm; CF_4, 0.5 ppm) are all either inert or in sufficiently low concentration so as to not perturb O atom profiles. Ultrahigh purity grade He (99.999%) for the resonance lamp and high-purity O_2 (99.995%) for the atomic filter were from AGA Gases. Scientific grade H_2 (99.9999%) and O_2 (99.999%), for reaction mixtures, were obtained from MG Industries. Analytical grade CH_3I (99%) and C_2H_5I (99%), both from Aldrich Chemical Co. Inc., were purified by bulb-to-bulb distillation, retaining only the middle thirds. Test gas mixtures were accurately prepared from pressure measurements using a Baratron capacitance manometer and were stored in an all-glass vacuum line.

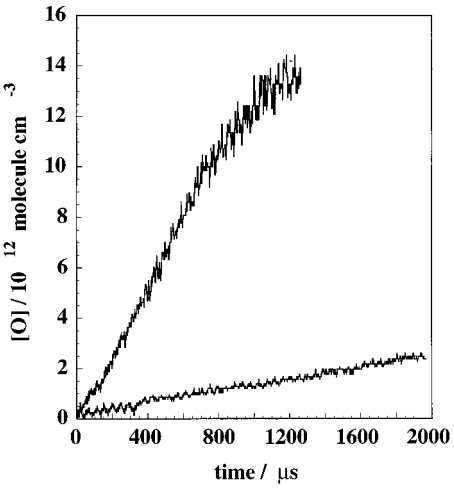

Figure 2. Measured O atom profiles for two typical experiments. The conditions for the upper trace are P_1= 10.99 Torr, M_s = 2.960, $X_{CH_3I} = 1.592 \times 10^{-6}$, and $X_{O_2} = 5.822 \times 10^{-2}$ giving T_5 = 2035 K, $\rho_5 = 2.594 \times 10^{18}$ molecules cm^{-3}, $[CH_3I] = 4.129 \times 10^{12}$ molecules cm^{-3}, and $[O_2] = 1.510 \times 10^{17}$ molecules cm^{-3}. For the lower trace, the conditions are P_1= 10.96 Torr, M_s = 2.597, $X_{CH_3I} = 1.592 \times 10^{-6}$, and $X_{O_2} = 5.822 \times 10^{-2}$ giving T_5 = 1608 K, $\rho_5 = 2.290 \times 10^{18}$ molecules cm^{-3}, $[CH_3I] = 3.645 \times 10^{12}$ molecules cm^{-3}, and $[O_2] = 1.333 \times 10^{17}$ molecules cm^{-3}.

Results

With the relatively high levels of O_2 used in this work, there is some resonance light absorption at 130 nm by O_2. Since this absorption is uniform over the O_2 bandwidth and $[O_2]$ does not change appreciably during an experiment, any observed transmittance decrease in the absence of CH_3I reflects both a total density increase due to vibrational relaxation of O_2 at low temperature and/or O atom formation from $O_2 + M \rightarrow 2O + M$ at high temperature. Under nearly identical conditions as the kinetics experiments, we corrected for both effects by carrying out several experiments without added CH_3I. The transmittance signals from the blanks were then point-by-point subtracted from the corresponding kinetics runs, leaving only the O atom formation signal from CH_3 oxidation. Relaxation time constants decreased with increasing temperature and were at most 250 μs near 1600 K. As expected, O atom formation increased with increasing temperature. However, the combination of both effects generally accounted for less than 20%; i.e., greater than 80% of the transmittance signal was due to O atom formation from CH_3 oxidation.

Using the corrected signals, $(ABS)_t$ was determined in each case and $[O]_t$ was calculated from the curve-of-growth shown in Figure 1. Figure 2 shows O atom profile results from two experiments, one at high temperature (2035 K) and the other at low temperature (1608 K). For both cases, $[CH_3I]_0 \cong 4 \times 10^{12}$ molecules cm^{-3}, and therefore, the available $[CH_3]$ is also 4×10^{12} molecules cm^{-3}. To understand these results and the results

TABLE 4: Mechanism Used for Fitting [O] Profiles from the $CH_3 + O_2$ Reaction[a]

1.	$CH_3I + Kr \rightarrow CH_3 + I + Kr$	$k_1 = 4.36 \times 10^{-9} \exp(-19858\ K/T)$[b]
2.	$CH_3 + O_2 \rightarrow H_2CO + OH$	$k_2 = 0$
3.	$CH_3 + O_2 \rightarrow CH_3O + O$	k_3 = fitted
4.	$CH_3O + Kr \rightarrow H_2CO + H + Kr$	$k_4 = 6.51 \times 10^{13} T^{-6.65} \exp(-16740\ K/T)$[c]
5.	$H + O_2 \rightarrow OH + O$	$k_5 = 1.62 \times 10^{-10} \exp(-7474\ K/T)$[d]
6.	$H_2CO + Kr \rightarrow HCO + H + Kr$	$k_6 = 1.019 \times 10^{-8} \exp(-38706\ K/T)$[e]
7.	$H_2CO + Kr \rightarrow H_2 + CO + Kr$	$k_7 = 4.658 \times 10^{-9} \exp(-32110\ K/T)$[e]
8.	$HCO + Kr \rightarrow H + CO + Kr$	$k_8 = 3.1 \times 10^{-7} T^{-1} \exp(-8555\ K/T)$[f]
9.	$HCO + O_2 \rightarrow HO_2 + CO$	$k_9 = 1.26 \times 10^{-11} \exp(-204\ K/T)$[g]
10.	$HO_2 + Kr \rightarrow H + O_2 + Kr$	$k_{10} = 2.0 \times 10^{-5} T^{-1.18} \exp(-24363\ K/T)$[c]
11.	$OH + OH \rightarrow O + H_2O$	$k_{11} = 7.19 \times 10^{-21} T^{2.7} \exp(1251\ K/T)$[d]
12.	$OH + H_2 \rightarrow H_2O + H$	$k_{12} = 3.56 \times 10^{-16} T^{1.52} \exp(-1736\ K/T)$[d]
13.	$OH + O \rightarrow O_2 + H$	$k_{13} = 5.42 \times 10^{-13} T^{0.375} \exp(1112\ K/T)$[d]
14.	$OH + H_2CO \rightarrow HCO + H_2O$	$k_{14} = 5.70 \times 10^{-15} T^{1.18} \exp(225\ K/T)$[h]
15.	$I + O_2 \rightarrow IO + O$	$k_{15} = 7 \times 10^{-11} \exp(-30977\ K/T)$[i]
16.	$H_2CO + O_2 \rightarrow HCO + HO_2$	k_{16} = fitted

[a] All rate constants are in cm^3 molecule^{-1} s^{-1}. [b] Reference 33. [c] References 1 and 35. [d] Reference 30. [e] Reference 36. [f] References 1 and 37. [g] References 1 and 38. [h] References 35 and 39. [i] Estimated from endothermicity.

from the other 16 experiments, it is necessary to numerically integrate an appropriate chemical mechanism to predict O atom profiles for the experimental conditions. It should be noted that the mechanism need not be all-inclusive, since the secondary chemistry cannot be highly perturbing because $[CH_3I]_0$ is so low.

Discussion

$[O]_t$ profiles of the 18 experiments in Table 3 were simulated using the mechanism of Table 4. However, considering only the initial stages of reaction where $[O]_t \leq 1 \times 10^{12}$ molecules cm^{-3}, initial profiles can be analytically determined if reactions 1, 4, and 5 can be considered to be instantaneous. For the conditions of the experiments, these are good assumptions. It is then easy to show that

$$[O]_t \cong \frac{2k_3[CH_3I]_0}{(k_2 + k_3)}\{1 - \exp(-(k_2 + k_3)[O_2]t)\} \qquad (7)$$

An initial estimate for k_3 can be made by expanding the exponential term giving $[O]_t \cong 2k_3[CH_3I]_0[O_2]t$. Hence, $k_3 \cong R_O/(2[CH_3I]_0[O_2])$ where R_O is the absolute O atom rate of formation (the initial slope) from profiles as illustrated in Figure 2. This approximate expression shows that no information about the branching ratio between reactions 2 and 3 can be obtained from initial O atom profile measurements alone.

Initial values of k_3 for all experiments were then determined using this approximate procedure. The results can be expressed in Arrhenius form as $k_3 \cong 2.4 \times 10^{-11} \exp(-16223\ K/T)$ cm^3 molecule^{-1} s^{-1}. Since CH_3 is depleting, this estimate will be a lower limit. Starting with the initial values for k_3, $[O]_t$ was then simulated with reactions 1−5 in Table 4. Some adjustments in k_3 were necessary, but under all conditions, initial profiles could be fitted. However, the simulations at longer times showed substantial negative deviations from experiment, particularly at high temperature. Obviously, reactions 1−5 of Table 4 are insufficient to explain the data, and the mechanism must be expanded.

We then attempted to use the full GRI mechanism[3] to explain the results. The high-temperature experiment shown in Figure 2 was numerically simulated,[40] and the predicted behavior is shown as open squares in Figure 3. Clearly, GRI-Mech 2.11 explains neither the initial rate of formation nor the long-time O atom yield. Similar calculations with the Leeds mechanism[41] are shown as the dotted line in Figure 3, and this mechanism

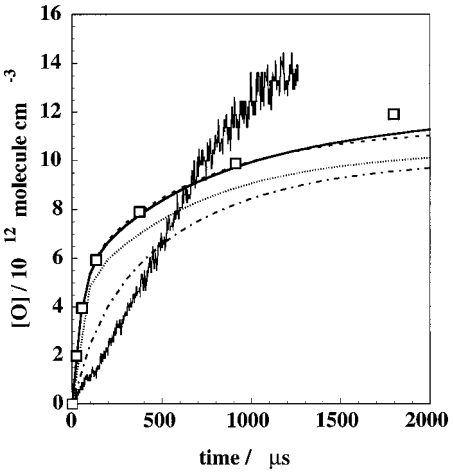

Figure 3. Comparison of the results for the 2035 K experiment of Figure 2 to numerical simulations as described in the text, with predictions using (□) the full GRI-Mech 2.11 mechanism (refs 3 and 40), (···) the Leeds mechanism (ref 41), (−) an irreversible 48 step reaction mechanism using some of the GRI rate constants, (- - -) the 16 step mechanism of Table 4 using some of the GRI rate constants, and (−·−·−·−) the 16 step mechanism of Table 4 using rate constants for reactions 2 and 3 from Yu et al. (ref 2).

also fails to reproduce the measurements. These mechanisms and the rate constants used in them are optimized against several experimental test cases and therefore cannot be modified in any way. Hence, neither code can be used for explaining the present data. We reduced the number of reactions considered in these mechanisms. By use of GRI-Mech rate constants, the solid line in Figure 3 is an irreversible 48 step reaction mechanism that includes CH_3 pyrolysis chemistry. Clearly, the reduction in mechanism size only affects the predictions at times greater than ∼1.5 ms. We reduced the mechanism even more to that shown in Table 4, and again with some of the GRI-Mech rate constants, the predictions (dashed line) are closely similar to the full GRI-Mech and reduced 48 step mechanisms. Last, we used the revised rate constants of Yu et al.[2] (eqs 4 and 5) for reactions 2 and 3, and the prediction is still disappointing, giving the dashed−dotted line in Figure 3. Their downward revision in both rate constants is still insufficient to explain the present data. It is obvious by inspection of Figure 3 that the initial O atom rate will require a rate constant for reaction 3 of about one-half that of eq 5, and this conclusion is reinforced by comparing our approximate k_3 to eq 5. The ratio is ∼0.3 over the present T range. It is also obvious from Figure 3 that the overall yield of O atoms at long times approaches $4[CH_3I]_0$,

suggesting that all three H atoms in CH_3 are somehow released to subsequently form O atoms in reaction 6. Reactions 1−5 in Table 4 only account for a maximum of two O atoms per initial CH_3, justifying the expanded 16 reaction mechanism of Table 4.

At low temperature, the kinetics are almost completely determined by reactions 1−5 of Table 4; however, as temperature increases, other processes can become important. It is important to assess the importance of reaction 2 (yielding $H_2CO + OH$) to the kinetics. As shown by eq 7, this reaction could have a substantial rate constant at low temperature and not affect the initial O atom rate from reaction 3. However, as temperature increases, the maximum O atom yield from reaction 2, followed by reactions 16, 8, 10, and 5 of Table 4, would be 2 O atoms per initial CH_3, and we measure yields approaching 4. With the Table 4 mechanism, inclusion of a substantial rate for reaction 2 that is competitive with our initial k_3 severely inhibits the total O yield. Any attempt to change the branching ratio to increase O atom production results in worse fits to the data, particularly at short times. The best fits are obtained with $k_2 = 0$ as shown in Table 4. The present results strongly suggest that reaction 2 is negligible, in essential agreement with the early assertion of Baldwin and Golden.[13]

The Table 4 mechanism has then been used to fit the 18 experiments of Table 3. To obtain the high measured yields, we have to postulate a fast direct reaction between H_2CO and O_2 giving HO_2 and HCO as products. In actual fact, the adopted 16 step mechanism is still too detailed for the small initial CH_3I used in the study. If reactions 9 and 11−15 are deleted, the [O] profile prediction is only decreased by less than 3%. Subsequent deletion of reactions 6 and 7 increases the prediction by about 12%, indicating some importance for H_2CO thermal decomposition. However, the most important subsequent reaction is the postulated reaction (i.e., reaction 16 in Table 4). Hence, the minimum mechanism for explaining the present data is reactions 1, 3−5, 8, 10, and 16 in Table 4. These, added together, give for complete conversion $CH_3 + 4O_2 = 3OH + 4O + CO$. By contrast, substituting reaction 2 for reaction 3, with the other processes contributing, gives $CH_3 + 3O_2 = 3OH + 2O + CO$. Hence, any study using OH-radical detection diagnostics will have difficulty in delineating which process, reaction 2 or 3, is important. However, the present O atom diagnostic method can be used to assess the relative importance.

Even though half of the reactions are unimportant, the entire 16 step mechanism in Table 4 was used to fit the data. The important rate constants (i.e., eqs 1, 3−5, 8, 10, and 16) are known with sufficient accuracy with the exception of reactions 3 and 16 in Table 4. Hence, the analysis really requires that both rate constants be iteratively changed until a satisfactory fit is obtained. The fits show (a) that $[CH_3]$ is depleted at all temperatures and (b) that reaction 16 is fast enough to slightly contribute to $[O]_t$ at relatively short times. Even though reaction 3 is almost isolated, reaction 16 has some effect. We find that initial rate estimates for eq 3 (i.e., $k_3 \cong 2.4 \times 10^{-11}$ $\exp(-16223\ \mathrm{K}/T)$ $\mathrm{cm^3\ molecule^{-1}\ s^{-1}}$) have to be only slightly increased (∼12%). The final values for k_3 are listed in Table 3. The values for reaction 16 are substantially less accurate at all temperatures because this process accounts for the additional [O] produced at longer times. The iteratively fitted values for the 18 experiments are listed in Table 3. Over the entire time ranges, the mutually derived values reproduce the O atom profiles to within ±10% for the experiments below 2000 K and to ±10−20% for those above 2000 K. The fits are satisfactory considering the ±10% accuracy of the O atom analysis using the COG from Figure 1. An example of a fit at $T = 2091$ K is shown in Figure 4.

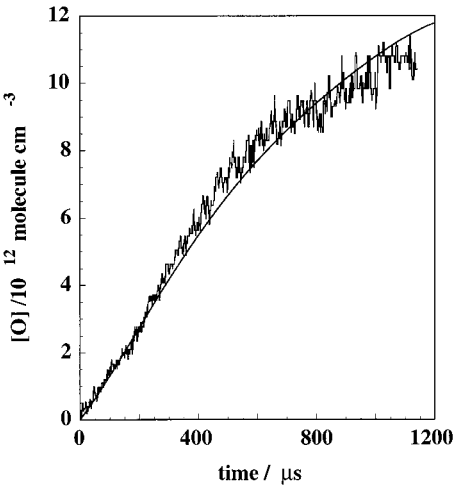

Figure 4. Comparison of a measured O atom profile for a typical high-temperature experiment to a simulation. The conditions are $P_1 = 10.93$ Torr, $M_s = 2.999$, $X_{CH_3I} = 1.592 \times 10^{-6}$, and $X_{O_2} = 5.822 \times 10^{-2}$, giving $T_5 = 2091$ K, $\rho_5 = 2.599 \times 10^{18}$ molecules $\mathrm{cm^{-3}}$, $[CH_3I] = 4.138 \times 10^{12}$ molecules $\mathrm{cm^{-3}}$, and $[O_2] = 1.513 \times 10^{17}$ molecules $\mathrm{cm^{-3}}$. The line is a fit using the mechanism of Table 4 together with the rate constants for reactions 3 and 16 given in Table 3.

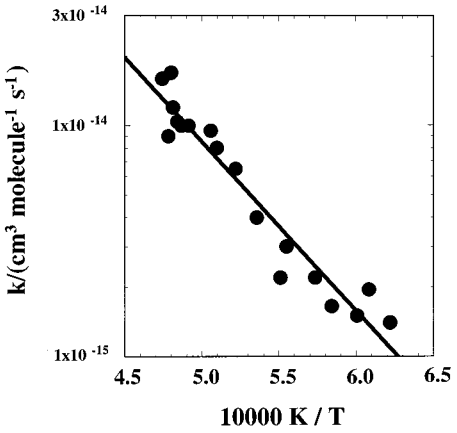

Figure 5. Arrhenius plot of the data for k_3 from Table 3. The line is given by eq 8, and the solid circles are the individual data points.

Arrhenius plots for reactions 3 and 16 in Table 4 are shown in Figures 5 and 6, respectively. Arrhenius analyses for the rate constants give

$$k_3 = (3.90 \pm 0.40) \times 10^{-11} \exp(-16858 \pm 1127\ \mathrm{K}/T)\ \mathrm{cm^3\ molecule^{-1}\ s^{-1}} \quad (8)$$

and

$$k_{16} = (4.82 \pm 0.72) \times 10^{-8} \exp(-28476 \pm 1628\ \mathrm{K}/T)\ \mathrm{cm^3\ molecule^{-1}\ s^{-1}} \quad (9)$$

and these expressions are plotted along with the data in Figures 5 and 6. Reaction 3 is nearly isolated and can be considered to be a direct determination; however, reaction 16 is secondarily derived and should only be considered to be consistent with the measurements.

The present determination for k_3 can be compared to earlier studies that are mentioned in the Introduction.[2,10,11,14−17,20,21] All results are higher by at least a factor of 2−3. The studies that

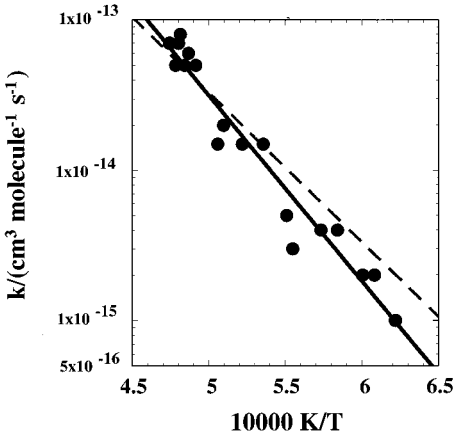

Figure 6. Arrhenius plot of the data from Table 3 for k_{16} of Table 4. The line is given by eq 9, and the solid circles are the individual data points. The dashed line is the approximate theoretical result given by eq 14.

are most similar to the present are those by Bhaskaran et al.[14] and Klatt et al.[17] who used O atom ARAS as the diagnostic. They report respective values

$$k_3 = 1.16 \times 10^{-11} \exp(-12900\ \mathrm{K}/T)\ \mathrm{cm}^3\ \mathrm{molecule}^{-1}\ \mathrm{s}^{-1} \quad (10)$$

and

$$k_3 = 3.80 \times 10^{-11} \exp(-15400\ \mathrm{K}/T)\ \mathrm{cm}^3\ \mathrm{molecule}^{-1}\ \mathrm{s}^{-1} \quad (11)$$

where both are valid over the present temperature range. Between 1600 and 2100 K, eq 10 is higher than eq 8 by a factor of 2−3 whereas eq 11 is higher by ∼2. We note that the present O atom ARAS technique is about 5 times more sensitive than those used earlier, and therefore, secondary reactions were more important in both earlier studies in contrast to the present where all radical−radical and many radical−molecule reactions are negligible. The most recent measurement from Braun-Unkhoff et al.[19] is

$$k_3 = 3.42 \times 10^{-12} \exp(-12242\ \mathrm{K}/T)\ \mathrm{cm}^3\ \mathrm{molecule}^{-1}\ \mathrm{s}^{-1} \quad (12)$$

and this result is higher than eq 8 by ∼50% at 1600 K but is lower by ∼25% at 2100 K. Hence, eq 12 is in fairly good agreement with the present result. The new result by Hwang, Ryu, De Witt, and Rabinowitz[42] is

$$k_3 = (2.66 \pm 0.78) \times 10^{-11} \exp(-15813 \pm 587\ \mathrm{K}/T)\ \mathrm{cm}^3\ \mathrm{molecule}^{-1}\ \mathrm{s}^{-1} \quad (13)$$

over the temperature range 1575−1822 K. This expression gives values only 31% and 22% higher than eq 8 at 1600 and 1800 K, respectively, and is therefore in excellent agreement with the present results.

There have been several theoretical investigations of reaction 3,[2,11,13,15,21,43] the most thorough being that of Yu et al.[2] On the basis of ab initio calculations[44,45] and derived models, they could explain the value for k_3, eq 5, determined in their study. We have not carried out theoretical calculations in this paper because fairly slight adjustments in their molecular structures, collisional efficiency factors, Lennard-Jones parameters, energetics, etc. could easily be made to justify the present value (about one-third of theirs). A more important question is whether reaction 2 has any experimental and/or theoretical support. These issues have also been discussed.[2,11,15,21,43,46,47] From a theoretical point of view, reaction 2 should be important if there is labile channel hopping between $CH_3O_2(^2A'')$ and $CH_3O_2(^2A')$. The $^2A''$ state correlates directly with reactants, $CH_3(^2A'') + O_2(^3\Sigma_g^-)$, and products, $CH_3O(^2E) + O(^3P)$, whereas the $^2A'$ state (estimated to be ∼20 kcal mol^{-1} above $^2A''$)[11,44,48] correlates with $CH_3(^2A'') + O_2(^1\Delta_g)$ (i.e., the first excited O_2 state) and with 1,3 hydrogen migration to form CH_2OOH and, ultimately, $H_2CO + OH$. Since the present work indicates little or no importance for reaction 2, we would conclude that either the crossing point is at higher energy than the direct process, reaction 3, or that state crossing is not labile.

To explain the profile results, reaction 16 of Table 4 has to have a large rate constant (eq 9). A relatively fast rate has previously been suggested by workers at lower temperatures between 700 and 900 K.[49,50] The question arises as to whether this reaction can be justified theoretically. Preliminary electronic structure calculations[51] indicate that $H_2CO(^1A_1) + O_2(^3\Sigma_g^-)$ correlates directly to $HCO(^2A') + HO_2(^2A'')$ through a loose $^3A''$ transition state. Presuming that the back process, HCO + HO_2, has little or no activation barrier, that for the forward process is then the zero-point-corrected endothermicity for the reaction, i.e., 38.94 kcal mol^{-1}. We note in the preliminary work[51] that there are two low-valued bending skeletal rocking frequencies that probably correlate with hindered rotations. We have therefore used these calculations to specify a loose transition state with two free internal rotors. Subsequent conventional transition-state theoretical (CTST) calculations with this model give to within ±0.8

$$k_{16}^{\mathrm{CTST}} = 7.785 \times 10^{-17} T^{2.049} \exp(-19089\ \mathrm{K}/T)\ \mathrm{cm}^3\ \mathrm{molecule}^{-1}\ \mathrm{s}^{-1} \quad (14)$$

for $300 \le T \le 2200$ K. Equation 14 is plotted in Figure 6 where it is seen to be in fair agreement with the data for reaction 16. Equation 14 also predicts values about 3−4 times greater than those reported by Baldwin et al.[50] between 713 and 816 K, and it gives values only about 2.5−5 times greater than GRI-Mech[3,52] over the temperature range 1350−2100 K. Since eq 14 is based on a preliminary unoptimized model, it cannot be considered to be accurate. However, the present demonstration suggests that such a process does have a theoretical basis and should be considered as probable.

Last, we are suggesting that there is a fast direct reaction between H_2CO and O_2, and there is a theoretical basis for this claim. Such a process has already been considered in shock tube H_2CO oxidation experiments by Eiteneer et al., who measured CO profiles;[52] however, a better demonstration would be to make direct O atom measurements on the H_2CO/O_2 system. Such experiments are planned in our laboratory in the near future. If fast rates for O atom formation are substantiated, these will be used to directly determine k_{16}, and the preliminary electronic structure calculations[51] will be refined and completed. This information will then be used in flexible transition-state theoretical calculations of thermal rate constants, thereby allowing for a direct comparison between experiment and theory.

Acknowledgment. The authors thank Drs. J. P. Hessler, A. F. Wagner, and Professor P. J. Ogren for carrying out modeling calculations and valuable discussions. We also thank Drs. D.-C. Fang and L. B. Harding for preliminary electronic structure calculations and Drs. S. M. Hwang and M. J. Rabinowitz for providing a prepublication version of their paper. This work was supported by the U.S. Department of Energy, Office of

Basic Energy Sciences, Division of Chemical Sciences, under Contract No. W-31-109-Eng-38.

References and Notes

(1) Mallard, W. G.; Westley, F.; Herron, J. T.; Hampson, R. F. *NIST Chemical Kinetics Database*, version 6.0; NIST Standard Reference Data; NIST: Gaithersburg, MD, 1994.

(2) Yu, C.-L.; Wang, C.; Frenklach, M. *J. Phys. Chem.* **1995**, *99*, 14377.

(3) Bowman, C. T.; Hanson, R. K.; Davidson, D. F.; Gardiner, W. C., Jr.; Lissianski, V.; Smith, G. P.; Golden, D. M.; Frenklach, M.; Goldenberg, M. GRI-Mech 2.11, http://www.me.berkeley.edu/gri_mech/.

(4) Dean, A. M.; Kistiakowsky, G. B. *J. Chem. Phys.* **1971**, *54*, 1718.

(5) Izod, T. P.; Kistiakowsky, G. B.; Matsuda, S. *J. Chem. Phys.* **1971**, *55*, 4425.

(6) Jachimowski, C. J. *Combust. Flame* **1974**, *23*, 233.

(7) Tsuboi, T. *Jpn. J. Appl. Phys.* **1976**, *15*, 159.

(8) Olson, D. B.; Gardiner, W. C., Jr. *Combust. Flame* **1978**, *32*, 151.

(9) Tabayashi, K.; Bauer, S. H. *Combust. Flame* **1979**, *34*, 63.

(10) Saito, K.; Ito, R.; Kakumoto, T.; Imamura, A. *J. Phys. Chem.* **1986**, *90*, 1422.

(11) Zellner, R.; Ewig, F. *J. Phys. Chem.* **1988**, *92*, 2971.

(12) Bowman, C. T. *Fifteenth Symposium (International) on Combustion*; The Combustion Institute: Pittsburgh, PA, 1975; p 869.

(13) Baldwin, A. C.; Golden, D. M. *Chem. Phys. Lett.* **1978**, *55*, 350.

(14) Bhaskaran, K. A.; Frank, P.; Just, Th. *Shock Tubes and Shock Waves*, *Proceedings of the Twelfth International Symposium on Shock Waves*; Lifshitz, A., Rom, R., Eds.; Magnes Press: Jerusalem, 1980; p 503.

(15) Teitelboim, M. A.; Vedeneev, V. I.; Goldenberg, N. Y.; Karnaukh, A. A. *Eleventh International Symposium on Gas Kinetics*; Assissi, Italy, 1990.

(16) Wu, C. H.; Lin, C.-Y.; Wang, H.-T.; Lin, M. C. In *Current Topics in Shock Waves*; Kim, Y. W., Ed.; Seventeenth International Symposium on Shock Waves and Shock Tubes, AIP Conference Proceedings 208; American Institute of Physics: New York, 1990; p 450.

(17) Klatt, M.; Röhrig, M.; Wagner, H. Gg. *Ber. Bunsen-Ges. Phys. Chem.* **1991**, *95*, 1163.

(18) Grela, M. A.; Amorebieta, V. T.; Colussi, A. J. *J. Phys. Chem.* **1992**, *96*, 7013.

(19) Braun-Unkhoff, M.; Naumann, C.; Frank, P. In *Shock Waves*; Brun, Raymond, Cumitrescu, Lucien, Eds.; Nineteenth International Symposium on Shock Waves; Springer: Berlin, Germany, 1995; Vol. 2, p 203.

(20) Brabbs, T. A.; Brokaw, R. S. *Fifteenth Symposium (International) on Combustion*; The Combustion Institute: Pittsburgh, PA, 1975; p 147.

(21) Dean, A. M.; Westmoreland, P. R. *Int. J. Chem. Kinet.* **1987**, *19*, 207.

(22) Tischer, A. L., IV; Hwang, S. M.; De Witt, K. J.; Rabinowitz, M. J. 1996 Fall Meeting of the Western States Section of the Combustion Institute, Stanford University, Stanford, CA; Paper 96F-124.

(23) Michael, J. V. *J. Chem. Phys.* **1989**, *90*, 189.

(24) Michael, J. V.; Sutherland, J. W. *Int. J. Chem. Kinet.* **1986**, *18*, 409.

(25) Michael, J. V.; Lim, K. P. *J. Chem. Phys.* **1992**, *97*, 3228.

(26) Maki, R. G.; Michael, J. V.; Sutherland, J. W. *J. Phys. Chem.* **1985**, *89*, 4815.

(27) Pamidimukkala, K. M.; Lifshitz, A.; Skinner, G. B.; Wood, D. R. *J. Chem. Phys.* **1981**, *75*, 1116.

(28) Kumaran, S. S.; Su, M.-C.; Lim, K. P.; Michael, J. V. *Twenty-Sixth Symposium (International) on Combustion*; The Combustion Institute: Pittsburgh, PA, 1996; p 605.

(29) Herzler, J.; Frank, P. *Ber. Bunsen-Ges. Phys. Chem.* **1992**, *96*, 1333.

(30) Michael, J. V. *Prog. Energy Combust. Sci.* **1992**, *18*, 327.

(31) Baulch, D. L.; Duxbury, J.; Grant, S. J.; Montague, D. C. *J. Phys. Chem. Ref. Data* **1981**, *10* (Suppl. 1).

(32) Lim, K. P.; Michael, J. V. *Twenty-Fifth Symposium (International) on Combustion*; The Combustion Institute: Pittsburgh, PA, 1994; p 713.

(33) Kumaran, S. S.; Su, M.-C.; Michael, J. V. *Int. J. Chem. Kinet.* **1997**, *29*, 535.

(34) Kumaran, S. S.; Michael, J. V. *Proceedings of the 21st International Symposium on Shock Waves*; Houwing, A. F. P., Ed.; Panther Publishing: Fyshwick, Australia, 1997; p 241.

(35) Tsang, W.; Hampson, R. F. *J. Phys. Chem. Ref. Data* **1987**, *15*, 1087.

(36) Kumaran, S. S.; Carroll, J. J.; Michael, J. V. *Twenty-Seventh Symposium (International) on Combustion*; The Combustion Institute: Pittsburgh, PA, 1998; p 125.

(37) Timonen, R. S.; Ratajczak, E.; Gutman, D.; Wagner, A. F. *J. Phys. Chem.* **1987**, *91*, 5324.

(38) Timonen, R. S.; Ratajczak, E.; Gutman, D. *J. Phys. Chem.* **1988**, *92*, 651.

(39) Baulch, D. L.; Cobos, C. J.; Cox, R. A.; Esser, C.; Frank, P.; Just, Th.; Kerr, J. A.; Pilling, M. J.; Troe, J.; Walker, R. W.; Warnatz, J. *J. Phys. Chem. Ref. Data* **1992**, *21*, 411.

(40) Hessler, J. P. Unpublished results using GRI-Mech 2.11.

(41) Pilling, M. J.; Turanyi, T.; Hughes, K. J.; Clague, A. R. The Leeds methane oxidation mechanism, version 1.3, http://www.chem.leeds.ac.uk/Combustion/Combustion.html.

(42) Hwang, S. M.; Ryu, S.-O.; De Witt, K. J.; Rabinowitz, M. J. *J. Phys. Chem.* **1999**, *103*, 5949.

(43) Benson, S. W. *Thermochemical Kinetics*; Wiley: New York, 1976.

(44) Walch, S. *Chem. Phys. Lett.* **1993**, *215*, 81.

(45) Sicilia, E.; DiMaio, F. P.; Russo, N. *Chem. Phys. Lett.* **1994**, *225*, 208.

(46) Ewig, F.; Rhasa, D.; Zellner, R. *Ber. Bunsen-Ges. Phys. Chem.* **1987**, *91*, 708.

(47) Hessler, J. P.; Du, H.; Ogren, P. J.; Wagner, A. F. 14th International Gas Kinetics Symposium, Leeds, UK, 1996; Paper F3.

(48) Hunziker, H. E.; Wendt, H. R. *J. Chem. Phys.* **1976**, *64*, 3488.

(49) Baldwin, R. R.; Langford, D.; Matchan, M. J.; Walker, R. W.; Yorke, D. A. *Thirteenth Symposium (International) on Combustion*; The Combustion Institute: Pittsburgh, PA, 1971; p 251.

(50) Baldwin, R. R.; Fuller, A. R.; Longthorn, D.; Walker, R. W. *J. Chem. Soc., Faraday Trans. 1* **1974**, *70*, 1257.

(51) Fang, D.-C.; Harding, L. B. Private communication, October, 1998.

(52) Eiteneer, B.; Yu, C.-L.; Goldenberg, M.; Frenklach, M. *J. Phys. Chem.* **1998**, *102*, 5196.